Ting Su, Yonghui Song*, Xinzhe Lan and Wenwen Gao

Adsorption optimized of the coal-based material and application for cyanide wastewater treatment

https://doi.org/10.1515/gps-2019-0006
Received June 20, 2018; accepted October 03, 2018.

Abstract: Custom design of JMP software was used to optimize the iodine number of coal-based electrode materials. Taking the additive ratio (A), heating rate (B) and final pyrolysis temperature (C) into account and the significance sequence was C>B>A. Set the additive ratio as 0.2, the heating rate as 5°C/min and the final temperature as 900°C, the iodine number was improved to 403.14 $mg \cdot g^{-1}$, and the compressive strength was 2.01 MPa. Surface morphology of the coal-based electrode materials were characterized by scanning electron microscopy (SEM). The functional group species were explored by Fourier infrared spectrophotometer (FTIR). Then applied the voltage of 4 V, coal-based adsorption materials were set as cathodes and anodes in a 3-dimensional electrode system with the commercial activated carbon as a particle electrode. After 5 h treatment for cyanide wastewater, the removal rate of most ions was achieved to 72% or more. It was the collaborative effect in the combined action of electro-adsorption and electrodeposition.

Keywords: coal-based material; JMP optimization; iodine number; cyanide wastewater; removal rate

List of abbreviations:

ad: air-dry basis;
M_{ad}: Moisture;
A_{ad}: Ash content;
V_{ad}: Volatiles;
FC_{ad}: Fixed Carbon;
C_{ad}: Carbon;
O_{ad}: Oxygen (by difference);
H_{ad}: Hydrogen;
N_{ad}: Nitrogen;
$S_{t,ad}$: total Sulfur;
$*FC_{ad} = 100\% - (V_{ad} + A_{ad} + M_{ad})$;
$*O_{ad} = 100\% - (C_{ad} + H_{ad} + N_{ad} + S_{ad} + A_{ad} + M_{ad})$;
CN_T: Total cyanide;
CN^-: Free cyanide;
SCN^-: Thiocyanate;
Cu: Cupper;
Zn: Zinc;
A: additive ratio;
B: heating rate;
C: final pyrolysis temperature;
CS: Compressive strength, MPa;
I_N: Iodine number, mg/g;
R^2: Correlation coefficient;
Φ: Diameter

1 Introduction

Due to the energy shortage and environmental pollution, renewable energy systems are suggested to play an increasing role in the industry and caused global concerns [1], especially the development of sustainable energy [2]. Carbon materials are widely explored as electrode materials because of their excellent electrical conductivity and outstanding electrochemical stability [3]. There are many advances in the synthesis of carbon electrode materials such as carbon nanofibers [4], carbon xerogels [5], carbon spheres [6], carbon nanosheets, carbon-metal oxide composites [7] and the activated carbon (AC) is the typical carbon electrode materials. The electrosorption of ions in aqueous solution by using AC as the electrode was studied in many works [8-11]. The coal, the petroleum coke, the wood, and the fruit shells can be the raw materials of carbon electrode materials [12]. Numerous researches [13-16] focused on the pyrolysis process of low-rank coal and oil shale, biomass, waste polymer plastics, coal liquefaction residue, and other organic materials. Due to this, it can be found that the features of AC give a high porous structure as well as an excellent conductivity. Combining the two properties, it can be prepared an excellent electrode for further applications, such as wastewater treatment. In order to

*** Corresponding author: Yonghui Song,** School of Metallurgical Engineering, Xi'an University of Architecture and Technology, Key Laboratory of Gold and Resources of Shaanxi Province, Xi'an, P.R. 710055, e-mail: syh1231@126.com
Ting Su and Xinzhe Lan, School of Metallurgical Engineering, Xi'an University of Architecture and Technology, Key Laboratory of Gold and Resources of Shaanxi Province, Xi'an, P.R. 710055
Ting Su and Wenwen Gao, School of Chemistry&Chemical Engineering, YuLin University, YuLin, P.R. 719000

Table 1: Proximate and ultimate analysis of SJC and DCLR.

Raw material	Proximate and Ultimate analysis/%								
	M_{ad}	A_{ad}	V_{ad}	$*FC_{ad}$	C_{ad}	$*O_{ad}$	H_{ad}	N_{ad}	$S_{t,ad}$
SJC	4.71	5.94	34.30	55.05	73.07	4.94	4.34	0.96	0.42
DCLR	1.15	10.42	32.24	56.19	78.59	3.26	4.22	0.99	1.26

discover the better electrosorption materials, using low-rank coal and coal liquefaction residue as raw materials in here to make a kind of coal-based electrode materials to treat the cyanide wastewater by electrosorption. However, how to obtain a better material becomes a challenge, because it depends on the ratio of materials, heating rate and final pyrolysis temperature. There are no available data reported in the literatures. Considering the experimental cost and efficacy, an effective experimental design is required. Therefore, the custom design of JMP software was adopted in this study. The software is not only to give a statistical analysis but also it can give a quadratic regression. Some powerful statistical methods were designed using JMP software to detect factors contributing to differences in many experiment processes. JMP software was widely used in experimental design in many disciplines such as metallurgy, medicine, management and materials science [17-20]. Once the materials were prepared at various conditions; characterization was needed. Highly positive correlations with methylene blue and iodine number were observed for AC adsorption capacity [21], in here, Iodine number was acted as an indicator representing the performance of coal-based adsorption materials.

2 Experimental methods

2.1 Materials

The low-rank coal from Sunjiacha (SJC) and the coal direct liquefaction residue (DCLR) were used as raw materials and additives respectively in this study. After de-ashing treatment of the DCLR, they were prepared by crushing, screening and drying at 110°C for 24 h in a vacuum drying oven. The quality percent of sample with particle sizes of less than 80 mesh was above 90%, two powder were mixed with set ratio and stirred with 500 rpm for 2 h. The proximate and ultimate analysis results of SJC and DCLR on an air-dry basis are presented in Table 1 and the ionic components of cyanide wastewater are shown in Table 2.

Table 2: Ionic components of cyanide wastewater (mg/L).

ion	CN_T	CN^-	Cu	Zn	SCN^-
Cyanide wastewater	1728.60	367.20	546.10	456.20	260.10

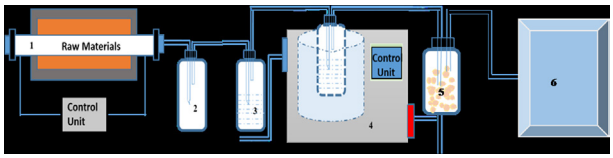

Figure 1: Schematic diagram of the experimental.
1-Vacuum tube-type furnace, 2-Air cooler, 3-First-water cooler, 4-Secondary water cooler, 5-Silica gel dying device, 6-Airbag

The characteristics of high volatile content and low sulfur as well as ash content of SJC are remarkable. The volatile content of DCLR reached at 32.24%, which was slightly lower than that of SJC. DCLR has a higher ash content of 10.42%. The chemical reaction of calcium, magnesium, aluminum, iron and other oxides in ash can affect the pore structure of the coal-based electrode material. Hydrogen content of two is more than 4.0%, and the distribution of hydrogen is directly related to the composition of pyrolysis gas. The porosity and pore size of coal-based electrode material were affected by the content and release rates of pyrolysis gas.

2.2 Furnace equipment

The mixed powder was formed to a coin like tablet with the size of Φ30 mm × 2 mm under a pressure of 8 MPa by FYD-40-A powder press machine, and the coal-based materials were allowed to air dry at room temperature for 24 h. Then the coal-based materials after pyrolysis process were treated with nitric acid (the wt% of coal-based materials and HNO_3 was 1:3) for 8 h and whereafter washed to neutrality and dried in oven at 80°C for 12 h to obtain the coal-based electrode materials. The Schematic diagram of the experimental is shown in Figure 1. Gas was dried before collected in a gas bag after air cooling plus double water cooling process.

2.3 Analysis and characterization

2.3.1 Yield and removal rate

The yields of pyrolysis without activation (ω), pyrolysis with activation (ω′) and the removal rate (φ) of ions were calculated from Eq. 1, 2 and 3.

$$\omega = \frac{m_2}{m_1} \times 100\% \quad (1)$$

$$\omega' = \frac{m_3}{m_2} \times 100\% \quad (2)$$

$$\varphi = \frac{C_0 - C_1}{C_0} \times 100\% \quad (3)$$

where m_1 is the quality of coal tablet, g; m_2 is the quality of coal tablet after pyrolysis process, g; m_3 is the quality of pyrolyzed coal electrode material after nitric acid activation, g; C_0 is the initial concentration of ions, mg/L; C_1 is the concentration of ions in post-adsorption liquid, mg/L.

2.3.2 Characterization

The compressive strength of coal-based electrode was tested by pellet electronic pressure tester LD-YB-2. Bruker VERTEX70 FTIR spectrometer was used to explore the function group of samples. The morphology of coal-based electrode materials was scanned by Carl Zeiss singma300 scanning Electron Microscopy (SEM).

2.4 Experimental design

Additive was used to assist in the formation of coal-based electrode materials, so a single factor experiment was carried out to learn the influence of the additive ratio (A) on the compressive strength (CS) and then determine the range of additive before response surface experiment design. The setting and compressive strength were shown in Table 3.

Higher CS was found at additive interval of 0.2-0.4. The response surface experiment design was carried out using the response surface design platform of JMP which is a data statistics software. Three parameters, including additive ratio, final pyrolysis temperature (B), heating rate (C), were studied and the setting of each parameter was shown in Table 4. In addition, a total of ten runs were listed in Table 5. Iodine number (I_N) was also shown in the last column of this table, which will be discussed later.

Table 3: The CS of coal-based electrode materials with different A (10°C/min, 800°C).

A	0.1	0.2	0.3	0.4	0.5
CS/MPa	1.24	1.83	1.89	1.76	1.37

3 Results and discussion

3.1 Iodine number

The iodine number of the coal-based electrode material was tested according to the test method for the iodine adsorption value of coal electrode material (GB/T 7702.7-2008). The coal-based electrode material require higher iodine number for better adsorption performance. The I_N values obtained were in the range of 262.74-376.08 mg/g, depending on the operating condition listed in Table 5. This indicates that the operating condition have an effect on the I_N value. However, the importance of parameter needs to be analysis further.

Table 4: Parameters and levels for the response surface design.

Parameter	Unit	−1	0	1
A	°C	0.2	0.3	0.4
B	–	700	800	900
C	°C · min^{-1}	5	10	15

Table 5: Experimental conditions conducted in this work.

No.	A	B	C	I_N
A-1	0.2	700	5	278.46
A-2	0.2	800	10	308.08
A-3	0.2	700	15	259.02
A-4	0.2	900	15	345.60
A-5	0.3	800	15	287.02
A-6	0.3	700	10	247.98
A-7	0.3	900	5	376.08
A-8	0.4	700	15	262.74
A-9	0.4	900	10	321.20
A-10	0.4	800	5	320.84

3.2 Yield of pyrolysis without activation and pyrolysis with activation

The yields of pyrolysis without activation were within the range of 68.8% to 75.9% in Figure 2a. According to the final temperature, the samples can be divided into 3 groups named high temperature group 1, medium temperature group 2 and low temperature group 3 respectively. The rules of higher final pyrolysis temperature caused the lower pyrolysis yield can be seen from these groups. With the higher final temperature, pyrolysis product will undergo secondary pyrolysis, which reduced the yield of pyrolysis solid product. Overall, the influence of temperature is important for the yield of pyrolysis. The pyrolysis yields with activation varied slightly within the range of 63.0% to 69.7% in Figure 2b. They were also divided into 3 groups and owned the same law as pyrolysis yield without activation. Meanwhile, with the increase of the additive ratio, the yield showed an increasing trend in each group. The sample of A-1 with the lowest yield of pyrolysis with activation but not the lowest pyrolysis yield without activation, indicating that the nitric acid erosion was very serious during the activation process, but it not means the porosity of A-1 was developed largely, The activation yield is not directly proportional to the pore development.

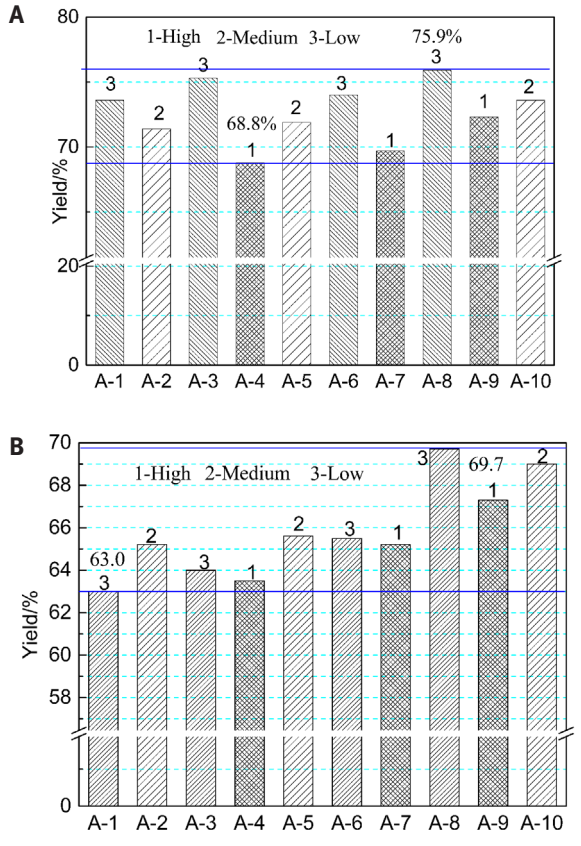

Figure 2: Yield of pyrolysis without activation (a) and pyrolysis with activation (b).

3.3 Compressive strength

The compressive strength of coal-based material is preferably above 1.5 MPa. The minimum value of 1.161 MPa was not available for electrode materials. Additive ratio increased from group 1 to group 3 in Figure 3, It was not shown the clearly relationship between the DCLR addition ratio and compressive strength value. The proportion of DCLR affected the compressive strength of the samples, but also affected by other factors at the same time.

3.4 Statistical analysis

The stepwise regression method was chosen to analyze the experimental data in Table 6. The quadratic regression surface model was established after eliminating the non-significant items. The model for Iodine number is calculated by the obtained quadratic regression equation given by Eq. 4.

$$I_N = 290.99 - 9.42X_1 + 42.76X_2 - 18.52X_3 + 7.32X_1^2 - 10.33X_1X_2 - 9.74X_2X_3 + 14.19X_3^2 \quad (4)$$

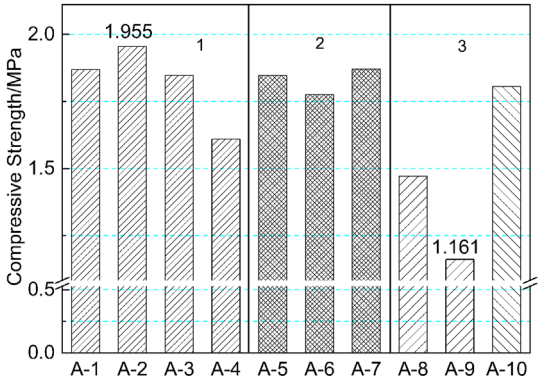

Figure 3: The compressive strength of samples.

Table 6: Analysis of variance for the regression model (R^2=0.9997).

source	Df	Sum of square	Mean square	F value	P-value
Model	8	15217.391	1902.17	4325.056	0.0118
Error	1	0.440	0.44		
Total	9	15217.831			

where: X_1, X_2, and X_3 are equal to (ratio-0.3)/0.1, (final temperature-800)/100 and (heating rate-10)/5.

According to the analysis of variance, this equation is suitable for expressing the model. The R^2=0.9997 and the low P-value (0.0118) indicated that the fitting models was reasonable. Hence, the model can be used to analyze and optimize the process parameters of coal-based electrode material.

In Table 7, the significant sequence for these key factors is X_2>X_3>X_1, the effects of the quadratic term X_1^2, X_1X_2, X_2X_3, X_3^2 on the number are also significant. This means that the final pyrolysis temperature is the most critical factor, and the interaction of three factors among them is not a simple linear relationship.

3.5 Optimization and verification

The above response surface quadratic model was applied to explore the best combination of three factors. The changes of iodine number with different selection of variables are shown in the predict profile as Figure 4.

According to the parameters in the prediction to obtain higher I_N of coal-based electrode materials, 3 parallel samples (A-11, A-12, A-13) were performed in laboratory and the iodine number was 398.70 mg·g^{-1}, 403.14 mg·g^{-1} and 401.22 mg·g^{-1} respectively, and the average I_N was 401.02 mg·g^{-1}, it was improved compared to before. The compressive strength of A-12 was 2.01 MPa, The properties of A-12 were analyzed by several methods in the following content.

Table 7: Significance test for the regression coefficients.

source	Df	Sum of square	F value	P-value
X_1	1	436.4298	992.3296	0.0202*
X_2	1	8977.7860	20413.19	0.0045*
X_3	1	1687.3849	3836.681	0.0103*
X_1^2	1	99.7850	226.8856	0.0422*
X_1X_2	1	370.3940	842.1810	0.0219*
X_1X_3	1	3.2252	7.3333	0.2252
X_2X_3	1	329.5877	749.3981	0.0232*
X_3^2	1	375.3104	853.3597	0.0218*

"*" means significant influence factor

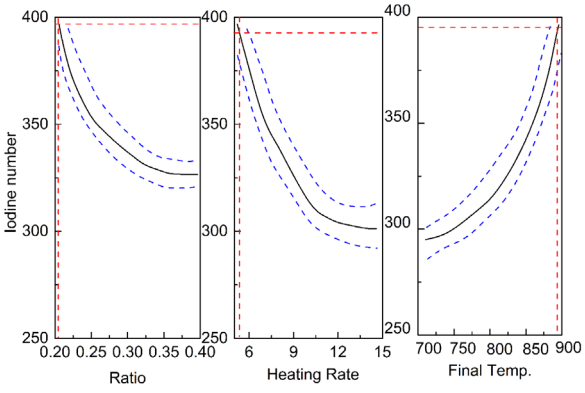

Figure 4: The predicted profile of higher I_N.

3.6 SEM analyze

No visible pore structure in the SEM image (Figure 5) of each sample except for Sample of A-12. The volatile of pyrolysis gas and the nitric acid erosion created and cleaned the pores. The main contribution of the iodine number comes from micropores. The pores in the 500-1000x SEM image are macropores. The higher iodine number of the A-12 should be the result of an increase in the number of micropores and macropores.

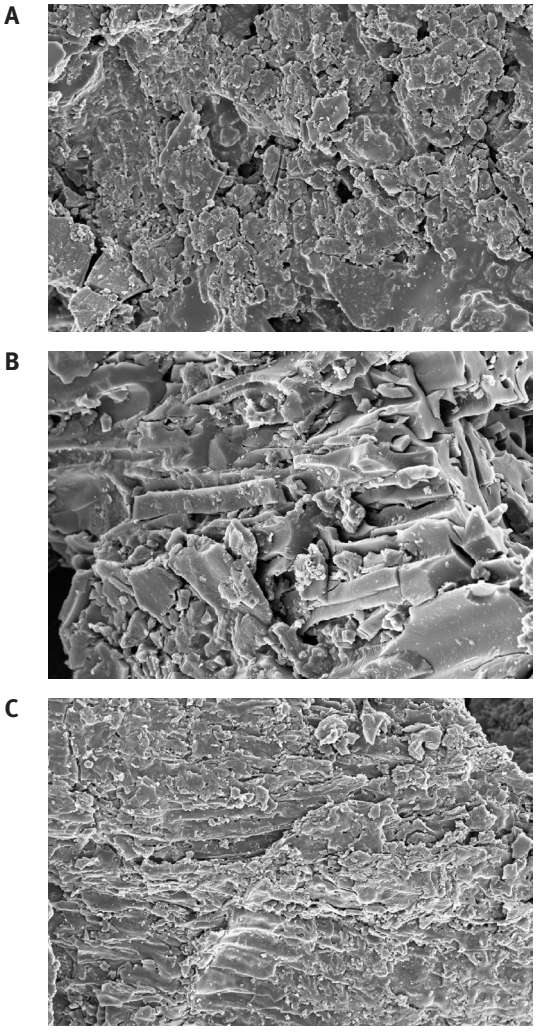

Figure 5: (Continued).

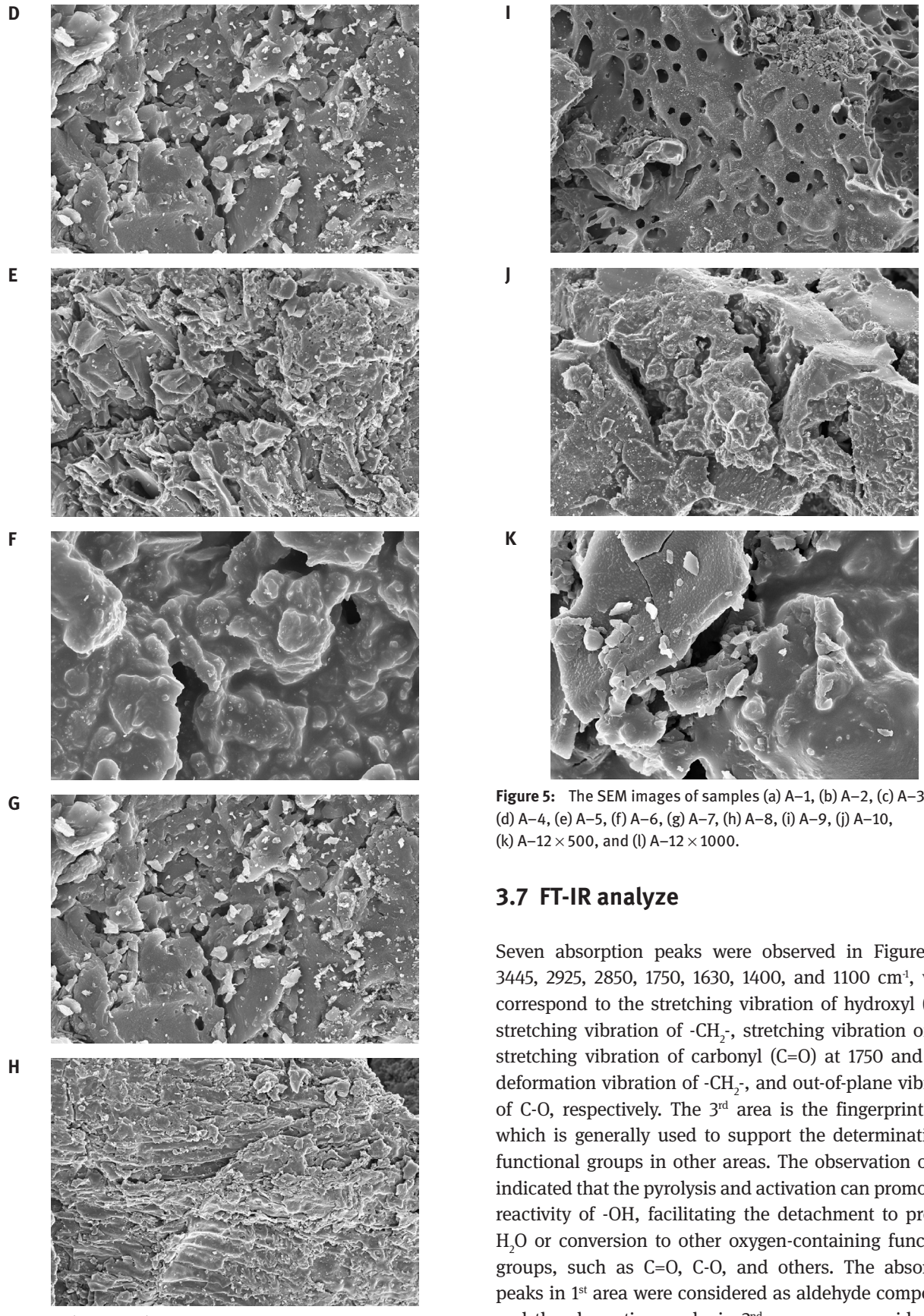

Figure 5: (Continued).

Figure 5: The SEM images of samples (a) A–1, (b) A–2, (c) A–3, (d) A–4, (e) A–5, (f) A–6, (g) A–7, (h) A–8, (i) A–9, (j) A–10, (k) A–12 × 500, and (l) A–12 × 1000.

3.7 FT-IR analyze

Seven absorption peaks were observed in Figure 6 at 3445, 2925, 2850, 1750, 1630, 1400, and 1100 cm^{-1}, which correspond to the stretching vibration of hydroxyl (-OH), stretching vibration of -CH_2-, stretching vibration of C-H, stretching vibration of carbonyl (C=O) at 1750 and 1630, deformation vibration of -CH_2-, and out-of-plane vibration of C-O, respectively. The 3rd area is the fingerprint area, which is generally used to support the determination of functional groups in other areas. The observation of -OH indicated that the pyrolysis and activation can promote the reactivity of -OH, facilitating the detachment to produce H_2O or conversion to other oxygen-containing functional groups, such as C=O, C-O, and others. The absorption peaks in 1st area were considered as aldehyde compounds and the absorption peaks in 2nd area were considered as

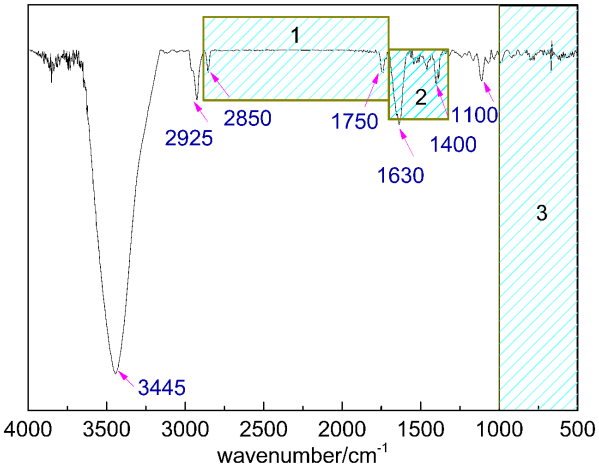

Figure 6: The FT-IR curve of coal-based electrode material.

aromatic compounds in this study. More oxygen-containing functional groups have better wettability and are beneficial for subsequent applications.

3.8 Pyrolysis mechanism

The pyrolysis process including several stages, the adsorbed H_2O, N_2 and CO_2 on the surface of the raw material were released at lower temperature. Several weak chemical bonds in SJC and DCLR began to break at higher temperature stage, resulting in a small amount of CO_2, N_2 and H_2O, also with some low-boiling substances. When the temperature raised to 400 °C-600 °C, an intense pyrolysis reaction occurred, and the number of colloids substantially increased. The colloids contain a large amount of asphaltene and preasphaltene, which were formed by hydrogen bonding between acid substances, such as phenolic hydroxyl groups, and alkaline substances, such as heterocyclic oxygen compounds or ether oxygen. When the gas volatilized from the coal matrix left the pore behind. And the pore structure improved the adsorption performance as well as the iodine number. The possible chemical reactions involved as follows (Ph/Ph′ means benzene ring).

$$Ph-CH_3 \rightarrow Ph-CH_2\cdot + H\cdot \quad (5)$$

$$Ph-O-Ph' \rightarrow Ph-O\cdot + Ph'\cdot \quad (6)$$

$$Ph-CH_2-Ph' \rightarrow Ph-CH_2\cdot + Ph'\cdot \quad (7)$$

$$Ph-CH_2-CH_3 \rightarrow Ph-CH_2\cdot + CH_3\cdot \quad (8)$$

$$Ph-O-CH_3 \rightarrow Ph-O\cdot + CH_3\cdot \quad (9)$$

$$Ph-O-CH_2-Ph' \rightarrow Ph-O-CH_2\cdot + Ph'-CH_2\cdot \quad (10)$$

Table 8: Removal rate of each ion in cyanide wastewater with voltage of 4V.

ion	CN_T	CN^-	Cu	Zn	SCN^-
concentration/(mg/g)	474.67	83.76	118.39	156.02	63.96
Removal rate/%	72.54	77.19	78.32	65.80	75.41

$$Ph-CH_2-CH_2-Ph' \rightarrow Ph-CH_3\cdot + Ph'-CH_2\cdot \quad (11)$$

3.9 Cyanide wastewater treatment

The coal-based electrode material was used as the anode and cathode, and the applied voltage was 4 V. Commercially activated carbon was used as a particle electrode, and the cyanide wastewater was treated in a three-dimensional electrode system for 5 h. Wastewater treatment experiment used three pieces of coal-based electrode sheets to form a double electric field effect. The results are shown in Table 8.

Seen from Table 8, the removal rate of each ion in the cyanide wastewater reached 72% or more except Zn ion. At voltages of 4 V, both electro-adsorption and electrodeposition existed in the system. Larger voltages give more driving forces to the ions. As long as the ion size matches the pore size of the coal-based electrode material, the adsorption removal effect can be achieved. At the same time, the oxidation-reduction reaction of the upper and negative anodes was the main source of deposition. Therefore, the removal rate of ion in the waste water is high, but the improvement is still needed, and further optimization is allowed in subsequent experiments.

4 Conclusions

Coal-based electrode materials were successfully prepared with the suitable addition ratio of SJC and DCLR. The final pyrolysis temperature was the most significant factor analyzed by JMP software. And the significance sequence was C > B > A. The interaction of parameters is found to be significant and needs to be considered in the empirical equation, giving an excellent estimation. The iodine adsorption value and compressive strength value of sample prepared with the optimized parameters was 403.14 mg·g^{-1} and 2.01 MPa respectively, giving a high porosity and a high surface area. The oxygen-containing functional groups on coal-based electrode materials were beneficial for wettability in order to treat the wastewater.

The removal rate of each ion in the three-dimensional electrode system was high. The removal rates of CN_T, CN^-, Cu, Zn, and SCN^- in wastewater were 72.54%, 77.19%, 78.32%, 65.80%, and 75.41%, respectively.

Acknowledgements: The authors acknowledge the financial support by Natural Science Foundation of Shaanxi Province of China (2019JM-542), National Natural Science Foundation of China (51774227), Natural Science Foundation of Shaanxi Province of China (2018JZ5011).

References

[1] Alaswad A., Baroutaji A., Achour H., Carton J., Al Makky A., Olabi A.G., Developments in fuel cell technologies in the transport sector. Int. J. Hydrogen Energy, 2016, 41(37), 16499-16508.

[2] Zhang L.L., Zhao X.S., Carbon-based materials as supercapacitor electrodes. Chem. Soc. Rev., 2009, 9, 2520-2531.

[3] Xu Y.X., Shi G.Q., Duan X.F., Self-assembled three-dimensional graphene macrostructures: synthesis and applications in supercapacitors. J. Acc. Chem. Res., 2015, 6, 1666-1675.

[4] Sheng J., Ma C., Ma Y., Zhang H.X., Wang R.R., Xie Z.Y., et al., Synthesis of microporous carbon nanofibers with high specific surface using tetraethyl orthosilicate template for supercapacitors. Int. J. Hydrogen Energy, 2016, 22, 9383-9393.

[5] Fernández P., Arenillas A., Calvo E., Menéndez J.A., Martins M.E., Carbon xerogels as electrochemical supercapacitors. Relation between impedance physicochemical parameters and electrochemical behavior. Int. J. Hydrogen Energy, 2012, 37, 10249-10255.

[6] Wickramaratne N.P., Xu J.T., Wang M., Zhu L., Dai L., Jaroniec M., Nitrogen enriched porous carbon spheres: attractive materials for supercapacitor electrodes and CO_2 adsorption. J. Chem. Mater., 2014, 26(9), 2820-2828.

[7] Yuan K., Hu T., Xu Y.Z., Graf R., Brunklas G., Forster M., et al., Engineering the morphology of carbon materials: 2D porous carbon nanosheets for high-performance supercapacitors. J. Chem. ElectroChem., 2016, 3, 822-828.

[8] Dai M., Xia L., Song S.X., Peng C.S., Rangel-Mendez J.R., Gaona R.C., Electrosorption of As(III) in aqueous solutions with activated carbon as the electrode. J. App. Surf. Sci., 2018, 434, 816-821.

[9] Park H., Choi J., Cheol Yang S., Han M.H., Kim D.K., Electrochemical characterization of electrolyte-filled porous carbon materials for electrosorption process. J. Electroanal. Chem., 2017, 801, 179-184.

[10] Li Y.Z., Jiang Y.P., Wang T.J., Zhang C., Wang H., Performance of fluoride electrosorption using micropore-dominant activated carbon as an electrode. J. Sep. Purific. Tech., 2017,172, 415-421.

[11] Wu P., Xia L., Dai M., Lin L.L., Song S.X., Electrosorption of fluoride on TiO_2-loaded activated carbon in water. J. Colloids Surfaces A: Physicochem. Eng. Aspects, 2016, 502, 66-73.

[12] Mirzaeian M., Abbas Q., Ogwu A., Hall P., Goldin M., Mirzaeian M., et al., Electrode and electrolyte materials for electrochemical capacitors. Int. J. Hydrogen Energy, 2017, 40, 25565-25587.

[13] Guo M., Cheng Bi J., Characteristics and application of co-pyrolysis of coal/biomass blends with solid heat carrier. J. Fuel Process. Tech., 2015, 138, 743-749.

[14] Bičáková O., Straka P., Co-pyrolysis of waste tire/coal mixtures for smokeless fuel, maltenes and hydrogen-rich gas production. J. Energy Convers. Manage., 2016, 116, 203-213.

[15] Wu Z.Q., Yang W.C., Tian X.Y., Yang B.L., Synergistic effects from co-pyrolysis of low-rank coal and model components of microalgae biomass. J. Energy Convers. Manage., 2017, 135, 212-225.

[16] Li B.F., Li X.H., Li W.Y., Feng J., Co-pyrolysis performance of coal and its direct coal liquefaction residue with solid heat carrier. J. Fuel Process. Tech., 2017, 166, 69-76.

[17] Ma H.Z., Yan C., Wang Y.N., Xie H.W., Statistical analysis and optimization of recovering indium from jarosite residure with vacuum carbothermic reduction by response surface methodology (RSM). J. Green Process. Synth., 2017, 6, 211-216.

[18] Fu M.K., Perlman M., Lu Q., Varga C., Pharmaceutical solid-state kinetic stability investigation by using moisture-modified Arrhenius equation and JMP statistical software. J. Pharm. Biomed. Anal., 2015, 107, 370-377.

[19] Qazi S., Samuel N.K., Venkatachalam T.K, Uckun F., Evaluating dissolution profiles of an anti-HIV agent using ANOVA and non-linear regression models in JMP software. Int. J. Pharm., 2003, 252(1-2), 27-39.

[20] Ye C., Liu J., Ren F.Y., Okafo N., Design of experiment and data analysis by JMP® (SAS institute) in analytical method validation. J. Pharm. Biomed. Anal., 2000, 23(2-3), 581-589.

[21] Qian H., Lin Y.L., Xu B., Wang L.P., Gao Z.C., Gao N.Y., Adsorption of haloforms onto GACs: Effects of adsorbent properties and adsorption mechanisms. Chem. Eng. J., 2018, 349, 849-859.